A Phase-Domain Synchronous Machine Model With Constant Equivalent Conductance Matrix for EMTP-Type Solution

Liwei Wang, *Member, IEEE*, and Juri Jatskevich, *Senior Member, IEEE*

(Invited Paper)

***Abstract*—Interfacing machine models in either nodal analysis-based (EMTP-like) or state variable-based transient simulation programs play an important role in numerical accuracy and computational performance of the overall simulation. As an advantageous alternative to the traditional qd models, a number of advanced phase-domain (PD) and voltage-behind-reactance machine models have been recently introduced. However, the rotor-position-dependent conductance matrix in the machine–network interface complicates the use of such models in EMTP. This paper focuses on achieving constant and efficient interfacing circuit for the PD synchronous machine model. It is shown that the machine conductance matrix can be formulated into a constant submatrix plus a time-variant submatrix. Eliminating numerical saliency from the second term results in a constant conductance matrix of the proposed PD model, which is a very desirable property for the EMTP solution since the refactorization of the network conductance matrix at every time step is avoided. Case studies demonstrate that the proposed PD model represents a significant improvement over other established models used in EMTP while preserving the accuracy of the original/classical PD model.**

***Index Terms*—Constant conductance matrix, EMTP, G matrix, phase-domain (PD) model, *qd* model, saliency elimination, synchronous machine, voltage-behind-reactance (VBR) model.**

NOMENCLATURE

Throughout this paper, bold font is used to denote matrix and vector quantities, and italic nonbold font is used to denote scalar quantities.

$\mathbf{v}_{abcs}, \mathbf{v}_{qdr}$	Stator and rotor voltage vectors.
$\mathbf{i}_{abcs}, \mathbf{i}_{qdr}$	Stator and rotor current vectors.
$\boldsymbol{\lambda}_{abcs}, \boldsymbol{\lambda}_{qdr}$	Stator and rotor flux linkage vectors.
$\mathbf{R}_s, \mathbf{R}_r$	Stator and rotor diag. resistance matrices.
$\mathbf{L}_s(\theta_r), \mathbf{L}_r$	Stator and rotor self-inductance matrices.
$\mathbf{L}_{sr}(\theta_r), \mathbf{L}_{rs}(\theta_r)$	Stator and rotor mutual-inductance matrices.
θ_r	Rotor position angle.
Δt	Discretization time step.
$\mathbf{R}_{\rm eq}^{pd}, \mathbf{G}_{\rm eq}$	Equivalent resistance and conductance matrices.
$\mathbf{e}_h^{pd}, \mathbf{i}_h^{pd}$	Equivalent history voltage and current sources.
$\mathbf{e}_{sh}^{pd}, \mathbf{e}_{rh}^{pd}$	Stator and rotor equivalent history sources.
Z_q'', Z_d''	Equivalent q- and d-axis subtransient impedances.
Z_{mq}, Z_{md}	Equivalent q and d-axis magnetizing impedances.
$Z_{lj}, j = kq1, \ldots kqM, fd, kd1, \ldots kdN$	Equivalent field and damper winding impedances.
Z_q'''	PD model modified q-axis subtransient impedance with added damper winding.
R_{kqM+1}, L_{lkqM+1}	Added damper winding resistance and leakage inductance.
Z_{lkqM+1}	Added damper winding impedance.
τ_{QM+1}	Added damper winding pole time constant.
$f_{\rm fit}$	Fitting frequency.
$L_{\rm critical}$	Critical leakage inductance for the added damper winding.

I. INTRODUCTION

MACHINE models for studying the power systems transients are generally based on the *qd*-axes model formulation. Such models have received extensive attention in the literature and are widely available in many nodal analysis-based electromagnetic transient programs (i.e., EMTP-type [1]) and state variable-based (e.g., Simulink [2]) simulation packages as built-in library components that are extensively used by many practicing engineers and researchers in industry and academia. Since such general purpose machine models are widely used, improving their numerical efficiency and accuracy can have significant impact and improve many simulation packages.

Manuscript received June 15, 2012; revised October 18, 2012; accepted November 9, 2012. Date of publication December 3, 2012; date of current version February 7, 2013. This work was supported in part by the Natural Sciences and Engineering Research Council of Canada under the Discovery Grant, and in part by the Educational Grant from BC Hydro. Paper no. TEC-00307-2012.

L. Wang is with ABB Corporate Research Center, Västerås SE-721 78, Sweden (e-mail: liwei.wang@se.abb.com).

J. Jatskevich is with the Department of Electrical and Computer Engineering, University of British Columbia, Vancouver, BC V6 T 1Z4, Canada (e-mail: jurij@ece.ubc.ca).

Color versions of one or more of the figures in this paper are available online at http://ieeexplore.ieee.org.

Digital Object Identifier 10.1109/TEC.2012.2227748

To improve the interface between the machine model and the external power system network, which is typically represented in physical abc phase coordinates, the so-called phase-domain (PD) [3]–[6] and voltage-behind-reactance (VBR) [7]–[9] models have been introduced. For numerically efficient interfacing of induction and synchronous machine models in state-variable transient simulation programs, a unified constant parameter *RL*-branch equivalent circuit has been recently proposed in [10].

Improving the numerical efficiency and accuracy of the synchronous machine models for the EMTP-type programs has been attractive for a long time. Numerous machine models have been proposed and implemented in various software packages including MicroTran [11], ATP/EMTP [12], PSCAD/EMTDC [13], and EMTP-RV [14], where the qd models are typically used. The main advantage of these methods is that they result in a constant machine conductance submatrix [18]. However, predicting relatively fast electrical variables introduces interfacing errors that significantly reduce the numerical accuracy of such models, and may potentially cause convergence problem [5], [8], [9]. In EMTP implementation, the advantages of PD and VBR synchronous machine models generally come at the price of having a rotor-position/speed-dependent machine conductance submatrix, which generally requires refactorization of the entire network conductance $\mathbf{G}$ matrix at every time step as the rotor position changes. A PD and VBR induction machine models that achieve constant conductance submatrix have been recently proposed by the authors in [15]. Achieving the same property for the VBR synchronous machine is very challenging due to the saliency and structure of equations [8]. Instead, the main focus and goal of this paper is to propose a new PD synchronous machine model that also achieves a constant conductance submatrix in EMTP solution, which, to the best of the authors' knowledge, has not been proposed before. Interested reader will find particularly useful the related work summarized in [8], [10], and [15]. The properties of the proposed PD model and the additional contributions of this paper are summarized as follows.

1) This paper shows that an equivalent resistance submatrix of the discretized PD synchronous machine model can be expressed as a constant plus a rotor-position-dependent term.
2) This property is used for deriving a model that has constant machine conductance submatrix as in [15] (assuming a magnetically linear machine) using approximation of saliency technique [16].
3) The proposed constant conductance (CC-PD) model can be achieved for either salient-pole or round rotor machines with appropriately fitted parameters for required accuracy and discretization time step.
4) The proposed CC-PD model is shown to maintain very good accuracy even at large time step similar to the classical PD model.

II. Coupled-Circuit PD Machine Model

For the purpose of power systems transients, a three-phase electrical machine can be modeled by lumped-parameter coupled circuits in physical variables and abc coordinates, known in EMTP community as the PD model. Without loss of generality, this paper considers a three-phase synchronous machine with one field winding fd, and M and N damper windings in the q- and d-axes, respectively. The parameters of the example machine considered in the case studies are summarized in Appendix A. All rotor windings are assumed to be referred to the stator side by appropriate turn ratios. Motor convention is used so that the stator currents flowing into the machine have a positive sign in the voltage equations. The flux linkage of each winding is assumed to have the same sign as the current flowing in that winding.

A. Continuous-Time PD Model

To set the stage for the further derivations, the PD model in continuous time is briefly included here. The voltage equation in physical variables and phase coordinates is [17]

$$\begin{bmatrix} \mathbf{v}_{abcs} \\ \mathbf{v}_{qdr} \end{bmatrix} = \mathbf{R} \begin{bmatrix} \mathbf{i}_{abcs} \\ \mathbf{i}_{qdr} \end{bmatrix} + p \begin{bmatrix} \boldsymbol{\lambda}_{abcs} \\ \boldsymbol{\lambda}_{qdr} \end{bmatrix} \tag{1}$$

where the resistance matrix is given as

$$\mathbf{R} = \begin{bmatrix} \mathbf{R}_s & \\ & \mathbf{R}_r \end{bmatrix}. \tag{2}$$

The flux linkage equation is expressed as

$$\begin{bmatrix} \boldsymbol{\lambda}_{abcs} \\ \boldsymbol{\lambda}_{qdr} \end{bmatrix} = \mathbf{L}(\theta_r) \begin{bmatrix} \mathbf{i}_{abcs} \\ \mathbf{i}_{qdr} \end{bmatrix} \tag{3}$$

where the stator and rotor self- inductance and mutual inductance matrix may be expressed as

$$\mathbf{L}(\theta_r) = \begin{bmatrix} \mathbf{L}_s(\theta_r) & \mathbf{L}_{sr}(\theta_r) \\ \mathbf{L}_{rs}(\theta_r) & \mathbf{L}_r \end{bmatrix}. \tag{4}$$

The detailed expressions of the resistance and inductance submatrices are given in Appendix B. The induced electromagnetic torque is calculated in terms of physical variables (currents) as follows:

$$T_e = \frac{P}{2}\left[\frac{1}{2}\mathbf{i}_{abcs}^T \frac{\partial}{\partial\theta_r}\left(\mathbf{L}_s - L_{ls}\mathbf{I}\right)\mathbf{i}_{abcs} + \mathbf{i}_{abcs}^T \frac{\partial \mathbf{L}_{sr}}{\partial\theta_r}\mathbf{i}_{qdr}\right] \tag{5}$$

which can be written in expanded form given in Appendix B, (B9) for simplified implementation instead of the involved matrix product (5). The mechanical equations can be found in [8] and [17], and are not included here due to space limitation.

B. Discretized PD Model for EMTP Solution

In order to obtain numerical solution within the EMTP, the PD machine model is discretized using implicit trapezoidal rule [1]. To interface the machine, the discretized model is first expressed in the following general form [8]:

$$\mathbf{v}_{abcs}(t) = \mathbf{R}_{\text{eq}}^{pd}\mathbf{i}_{abcs}(t) + \mathbf{e}_h^{pd}(t) \tag{6}$$

where the equivalent resistance matrix $\mathbf{R}_{\text{eq}}^{pd}$ is expressed as

$$\mathbf{R}_{\text{eq}}^{pd}(t) = \mathbf{R}_s + \frac{2}{\Delta t}\mathbf{L}_s(t) - \frac{4}{\Delta t^2}\mathbf{L}_{sr}(t)\left(\mathbf{R}_r + \frac{2}{\Delta t}\mathbf{L}_r\right)^{-1}\mathbf{L}_{rs}(t). \quad (7)$$

The history term $\mathbf{e}_h^{pd}(t)$ is represented as

$$\mathbf{e}_h^{pd}(t) = \mathbf{e}_{sh}^{pd}(t) + \frac{2}{\Delta t}\mathbf{L}_{sr}(t)\left(\mathbf{R}_r + \frac{2}{\Delta t}\mathbf{L}_r\right)^{-1} \times (\mathbf{v}_{qdr}(t) - \mathbf{e}_{rh}^{pd}(t)). \quad (8)$$

where

$$\mathbf{e}_{sh}^{pd}(t) = \left(\mathbf{R}_s - \frac{2}{\Delta t}\mathbf{L}_s(t-\Delta t)\right)\mathbf{i}_{abcs}(t-\Delta t) - \frac{2}{\Delta t}\mathbf{L}_{sr}(t-\Delta t)\mathbf{i}_{qdr}(t-\Delta t) - \mathbf{v}_{abcs}(t-\Delta t) \quad (9)$$

and

$$\mathbf{e}_{rh}^{pd}(t) = \left(\mathbf{R}_r - \frac{2}{\Delta t}\mathbf{L}_r\right)\mathbf{i}_{qdr}(t-\Delta t) - \frac{2}{\Delta t}\mathbf{L}_{rs}(t-\Delta t)\mathbf{i}_{abcs}(t-\Delta t) - \mathbf{v}_{qdr}(t-\Delta t). \quad (10)$$

The rotor currents can be expressed as

$$\mathbf{i}_{qdr}(t) = \left(\mathbf{R}_r + \frac{2}{\Delta t}\mathbf{L}_r\right)^{-1}\left(\mathbf{v}_{qdr}(t) - \frac{2}{\Delta t}\mathbf{L}_{rs}(t)\mathbf{i}_{abcs}(t) - \mathbf{e}_{rh}^{pd}(t)\right). \quad (11)$$

In the machine interface equation (6), the equivalent resistance matrix $\mathbf{R}_{\text{eq}}^{pd}$ is of our particular interest. Based on (7), it is observed that $\mathbf{R}_{\text{eq}}^{pd}$ is the sum of three terms: the stator resistance matrix $\mathbf{R}_s$, the stator inductance matrix term $\frac{2}{\Delta t}\mathbf{L}_s(t)$, and the third term: the triple matrix product of $-\frac{4}{\Delta t^2}\mathbf{L}_{sr}(t)$ $(\mathbf{R}_r + \frac{2}{\Delta t}\mathbf{L}_r)^{-1}\mathbf{L}_{rs}(t)$. It is shown in [15] that for induction machines, due to machine's symmetry, the second and third terms are independent of the rotor displacement θ_r. Therefore, matrix $\mathbf{R}_{\text{eq}}^{pd}$ is constant for symmetrical induction machines (assuming magnetic saturation is ignored).

In the case of synchronous machines, the stator inductance matrix $\mathbf{L}_s(t)$ is rotor-position-dependent due to salient-pole rotor. The third term, $\frac{4}{\Delta t^2}\mathbf{L}_{sr}(t)(\mathbf{R}_r + \frac{2}{\Delta t}\mathbf{L}_r)^{-1}\mathbf{L}_{rs}(t)$, in (7) is also rotor-position-dependent since the machine's geometry and winding parameters in q- and d-axis are no longer the same as in induction machines.

However, as it turns out (see Appendix C, Theorem 1) that for the synchronous machine with salient or round rotor, the equivalent resistance matrix (7) can be expressed as a constant plus a rotor-position-dependent part, as follows:

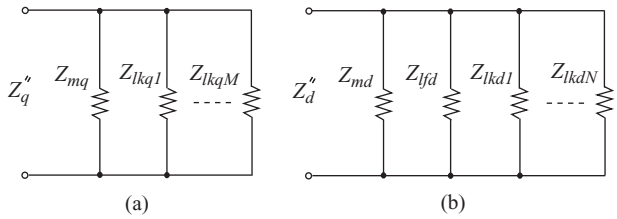

Fig. 1. Equivalent subtransient impedances in discrete-time domain: (a) q-axis, Z_q''; and (b) d-axis, Z_d''.

$$\mathbf{R}_{\text{eq}}^{pd}(t) = \mathbf{R}_0 + \frac{1}{3}\left(Z_q'' - Z_d''\right) \times \begin{bmatrix} \cos 2\theta_r & \cos 2\left(\theta_r - \frac{\pi}{3}\right) & \cos 2\left(\theta_r + \frac{\pi}{3}\right) \\ \cos 2\left(\theta_r - \frac{\pi}{3}\right) & \cos 2\left(\theta_r - \frac{2\pi}{3}\right) & \cos 2\theta_r \\ \cos 2\left(\theta_r + \frac{\pi}{3}\right) & \cos 2\theta_r & \cos 2\left(\theta_r + \frac{2\pi}{3}\right) \end{bmatrix} \quad (12)$$

where $\mathbf{R}_0$ represents the constant part. Moreover, in (12), the equivalent discrete-time q- and d-axis subtransient impedances Z_q'' and Z_d'' are defined as

$$Z_q'' = \left((Z_{mq})^{-1} + \sum_{i=1}^{M}(Z_{lkqi})^{-1}\right)^{-1} \quad (13)$$

$$Z_d'' = \left((Z_{md})^{-1} + (Z_{lfd})^{-1} + \sum_{i=1}^{N}(Z_{lkdi})^{-1}\right)^{-1} \quad (14)$$

with

$$Z_{mq} = \frac{2}{\Delta t}L_{mq} \text{ and } Z_{md} = \frac{2}{\Delta t}L_{md} \quad (15)$$

and

$$Z_{lj} = R_j + \frac{2}{\Delta t}L_{lj}, \quad \text{where } j = kq1, \ldots kqM, fd, kd1, \ldots kdN. \quad (16)$$

The equivalent circuits depicting the discrete-time domain subtransient impedances Z_q'' and Z_d'' are illustrated in Fig. 1. In general, the term $Z_q'' - Z_d''$ in (12) is nonzero for either round or salient rotor machines and it is not to be confused with dynamic or rotor saliency of the machine. However, this numerical saliency, $Z_q'' \neq Z_d''$ in (12), makes matrix $\mathbf{R}_{\text{eq}}^{pd}$ also rotor-position-dependent. By analogy, the unequal q- and d-axes subtransient inductances/reactances make the equivalent inductance matrix rotor-position-dependent in the continuous time synchronous machine VBR model [7].

III. Constant Equivalent Conductance Matrix

To interface the machine model with the external EMTP network, the machine branch voltages (6) are replaced by the nodal

equation as

$$\mathbf{G}_{\rm eq}\mathbf{v}_{abcs} = \mathbf{i}_{abcs} + \mathbf{i}_h^{pd}. \tag{17}$$

Here, the equivalent conductance matrix is calculated as

$$\mathbf{G}_{\rm eq} = [\mathbf{R}_{\rm eq}^{pd}]^{-1}. \tag{18}$$

This 3×3 submatrix $\mathbf{G}_{\rm eq}$ is then inserted into the overall network conductance matrix $\mathbf{G}$, which forms the standard nodal equation, $\mathbf{G}\mathbf{V}_n = \mathbf{I}_h$. The machine history current sources, $\mathbf{i}_h^{pd} = \mathbf{G}_{\rm eq}\mathbf{e}_h^{pd}$, is then injected into the nodes corresponding to the machine terminals (appropriately included into $\mathbf{I}_h$). Moreover, for an efficient EMTP solution, it is desirable to have matrix $\mathbf{G}$ constant [1]. The main focus of this section is to achieve a constant machine equivalent conductance matrix $\mathbf{G}_{\rm eq}$ for the conventional PD models [4], [5], [8].

A. Elimination of Numerical Saliency

The approach of removing this numerical saliency in (12) is based on a pioneering technique introduced in [16], which adds one additional artificial damper winding to one of the axis with the purpose of achieving a certain numerical property. Otherwise, this additional winding has no physical significance or relationship to the actual machine parameters. In particular, depending on the relative values of Z_q'' and Z_d'', the artificial winding should be added to the axis with the highest discrete-time domain subtransient impedance. Observing that the winding parameters in (13) and (14) are asymmetrical, it is typical that the d-axis has the lowest impedance (see [10]). Without loss of generality, it is assumed that a new $M+1$ damper winding with resistance R_{kqM+1} and leakage inductance L_{lkqM+1} is added to the q-axis. To distinguish the subtransient quantities of the new model that uses the $(M+1)$th winding, and for consistency with [10], we use the triple-prime sign ($'''$) instead of double-prime sign ($''$). The new equivalent subtransient impedance in the q-axis, including the added winding, becomes

$$Z_q''' = \left((Z_{mq})^{-1} + \sum_{i=1}^{M} (Z_{lkqi})^{-1} + (Z_{lkqM+1})^{-1} \right)^{-1} \tag{19}$$

where

$$Z_{lkqM+1} = R_{kqM+1} + \frac{2}{\Delta t} L_{lkqM+1}. \tag{20}$$

The parameters R_{kqM+1} and L_{lkqM+1} should be carefully selected such that

$$Z_q''' = Z_d''. \tag{21}$$

Condition (21) removes the rotor-position-dependent term in (12) and gives the desired result:

$$\mathbf{G}_{\rm eq} = [\mathbf{R}_{\rm eq}^{pd}]^{-1} = [\mathbf{R}_0]^{-1} = \text{constant}. \tag{22}$$

The new constant conductance phase-domain (CC-PG) model is then implemented similar to the conventional PD model [8], except that $\mathbf{R}_{\rm eq}^{pd}$ and $\mathbf{G}_{\rm eq}$ are calculated only once using (7) and (22).

B. Calculation of Added Winding Parameters

It is noted that discrete-time domain impedances Z_q'' and Z_d'' are dependent on the machine parameters (resistances and inductances) as well as the discretization time step Δt [see (13)–(16)]. Therefore, based on (13), (14) and (20), (21), the added winding equivalent impedance in discrete time can be calculated as

$$Z_{lkqM+1} = [(Z_d'')^{-1} - (Z_q'')^{-1}]^{-1}. \tag{23}$$

However, (23) and (20) do not uniquely define the finding parameters for a given time step Δt. Moreover, as it has been shown in [16], adding this extra damper winding also changes the q-axis operational impedance by adding a corresponding pole (and zero) to the respective transfer function [17, Ch. 7]. In order to preserve a good accuracy in predicting the machine's transients, it is important to select the additional winding parameters such that the low-frequency response is preserved, and the effect of extra winding may appear visible only in high frequencies that are above the range of interest—fit frequency, $f_{\rm fit} \approx 120$ Hz [16]. Assuming the same guidelines as in [16], the added pole time constant should be placed about ten times higher than the fit frequency. That is

$$\tau_{QM+1} \leq \frac{1}{2\pi \cdot 10 f_{\rm fit}}. \tag{24}$$

Furthermore, using the analysis of machine time constants [17, Ch. 7], the corresponding time constant can be also calculated as

$$\tau_{QM+1} = \frac{L_{lkqM+1}}{R_{kqM+1}} + \frac{1}{R_{kqM+1}} \left((L_{mq})^{-1} + \sum_{i=1}^{M} (L_{lkqi})^{-1} \right)^{-1}. \tag{25}$$

Combining (24) and (25), we get

$$R_{kqM+1} \geq 20\pi \cdot f_{\rm fit} \cdot L_{lkqM+1} + 20\pi \cdot f_{\rm fit} \cdot \left((L_{mq})^{-1} + \sum_{i=1}^{M} (L_{lkqi})^{-1} \right)^{-1}. \tag{26}$$

Substituting (26) into (20), we can define a critical value for the leakage inductance as

$$L_{\rm critical} = \frac{Z_{lkqM+1} - 20\pi \cdot f_{\rm fit} \cdot \left((L_{mq})^{-1} + \sum_{i=1}^{M} (L_{lkqi})^{-1} \right)^{-1}}{20\pi \cdot f_{\rm fit} + 2/\Delta t}. \tag{27}$$

Thereafter, the additional winding leakage inductance and resistance are calculated as follows:

$$L_{lkqM+1} \leq L_{\rm critical} \tag{28}$$

$$R_{kqM+1} = Z_{lkqM+1} - \frac{2}{\Delta t} L_{lkqM+1}. \tag{29}$$

For the purpose of this paper, it was assumed that $L_{lkqM+1} = L_{\rm critical}$. The corresponding parameters calculated for different time steps are included in Appendix A.

IV. Model Computational Efficiency Analysis

In order to achieve fastest possible simulation speed, the numerical implementation of the machine model has to be carefully optimized. For the conventional PD and CC-PD models considered in this paper, we consider all possible computational savings, including efficient calculation of trigonometric functions and utilization of symmetrical properties of machine matrices. It is observed in Section II and Appendix B that PD models require evaluation of trigonometric functions for the calculation of resistance matrix, history terms, and electromagnetic torque. More specifically, the models need evaluating $\cos(2\theta_r)$ and $\cos(2\theta_r \pm 2\pi/3)$ terms in $\mathbf{L}_s(\theta_r)$; then terms $\sin(\theta_r), \sin(\theta_r \pm 2\pi/3), \cos(\theta_r \pm 2\pi/3)$ in $\mathbf{L}_{sr}(\theta_r)$; and $\sin(2\theta_r)$ in $T_e(\theta_r)$. The evaluation of trigonometric functions depends on many factors, including the CPU hardware and low-level software implementation of trigonometric functions on a specific computer platform. Usually, high-order polynomial approximation or lookup table methods are used to evaluate these functions [19]. For example, the studies conducted on a typical Intel-based PC with Microsoft Windows Operating System show that evaluation of a single trigonometric function may cost about twenty equivalent flops, where one flop is defined as one addition, subtraction, multiplication, or division of two floating-point numbers [20].

As the evaluation of trigonometric functions is in general more expensive than performing simple additions and multiplications, efficient use of trigonometric functions is important. In this paper, an efficient calculation of the required trigonometric functions is implemented similar to the method used in [21]. Specifically, instead of calculating these functions directly by calling $\cos(\cdot)$ and $\sin(\cdot)$ each time for different arguments, only two functions $\cos(\theta_r)$ and $\sin(\theta_r)$ for a given angle θ_r are evaluated. Thereafter, the remaining trigonometric functions are calculated indirectly using identities:

$$\cos(2\theta_r) = 2\cos^2\theta_r - 1 \tag{30}$$

$$\sin(2\theta_r) = 2\cos\theta_r \sin\theta_r \tag{31}$$

$$\cos(2\theta_r \pm 2\pi/3) = -1/2\cos 2\theta_r \mp \sqrt{3}/2\sin 2\theta_r \tag{32}$$

$$\cos(\theta_r \pm 2\pi/3) = -1/2\cos\theta_r \mp \sqrt{3}/2\sin\theta_r \tag{33}$$

$$\sin(\theta_r \pm 2\pi/3) = -1/2\sin\theta_r \pm \sqrt{3}/2\cos\theta_r. \tag{34}$$

Evaluation of trigonometric functions using (30)–(34) requires much less computational efforts compared with the direct evaluation of these functions. For example, the required number of equivalent flops using both direct and indirect approaches is summarized in Table I. Since indirect calculation achieves significant computational savings, it is therefore considered in the final implementation of both conventional PD and CC-PD models.

Next, the computational costs of PD and CC-PD models are compared in terms of flop counts for a single time step. A typical salient-pole hydroturbine synchronous machine is used wherein the machine parameters are given in Appendix A and [17]. The considered generator model has the field winding *fd*, and two damper windings, *kd* and *kq1*, respectively. The CC-PD model is formulated according to Section III with one additional damper winding *kq2* in q-axis. Thus, the dimension of the rotor matrices and variables in the CC-PD model is higher than those in the original PD model. To maximize the numerical efficiency of both models, all constant terms and coefficient are precalculated outside of the main time stepping loop of the simulation. For example, the constant coefficients in the machine resistance matrix (12) are precalculated before the time step loop. For efficient calculation of electromagnetic torque in PD models, instead of the direct calculation using (5), the expanded form of torque equation (B9) in Appendix B is used. This reduces the number of flops since the two triple matrix products in (5) are avoided and minimizes the additional flops due to the added damper winding (see Table II).

After utilization of the efficient method for evaluation of trigonometric functions described in this section, the total numbers of flops required by the PD and CC-PD models are summarized in Table II. For better comparison and understanding of the computational costs, the flops are roughly assigned to several terms of the respective models. It is observed in Table II that the CC-PD model requires no flops for the evaluation of $\mathbf{R}_{\rm eq}$ in time stepping loop. However, the calculation of history term $\mathbf{e}_h$ and rotor current $\mathbf{i}_{qdr}$ make the constant CC-PD model

TABLE I
Comparison of Trig Functions Implementations

Method	Direct	Indirect
Functions	$\cos\theta$, $\sin\theta$ $\cos(2\theta)$, $\sin(2\theta)$ $\cos(2\theta \pm 2\pi/3)$ $\cos(\theta \pm 2\pi/3)$ $\sin(\theta \pm 2\pi/3)$	$\cos\theta$, $\sin\theta$ plus additional operations $10\otimes + 7\oplus$
Total cost	10 trigs + 5 flops	2 trigs + 17 flops
Equiv. flops	205	57

Here $\otimes$ and $\oplus$ denote multiplication and addition/subtraction operations.

TABLE II
Flops and Trig Functions Count per Time Step

Conventional PD Model			CC-PD Model		
$\mathbf{L}_s(\theta_r)$ $\mathbf{L}_{sr}(\theta_r)$ $\mathbf{L}_{rs}(\theta_r)$	flop	trig	$\mathbf{L}_s(\theta_r)$ $\mathbf{L}_{sr}(\theta_r)$ $\mathbf{L}_{rs}(\theta_r)$	flop	trig
	33	2		33	2
$\mathbf{R}_{eq}^{PD}$	9	-	$\mathbf{R}_{eq}^{CC-PD}$	0	-
$\mathbf{e}_h^{PD}$	90	-	$\mathbf{e}_h^{CC-PD}$	130	-
$\mathbf{i}_{qdr}^{PD}$	29	-	$\mathbf{i}_{qdr}^{CC-PD}$	41	-
T_e^{PD}	50	-	T_e^{CC-PD}	51	-
Total	211	2	Total	255	2
Equiv. flops	251		Equiv. flops	295	

slightly more costly than the conventional PD model due to the higher dimension of the rotor matrices and one extra rotor current. As a result, the CC-PD model requires more flops per time step compared to the conventional PD model (295 flops versus 251 flops).

V. Case Studies

Since the main idea of this paper is about the new CC-PD machine model rather than the power network solution, and due to the limited space, the presented studies and discussion are focused on a synchronous-machine infinite-bus system. The proposed model has been implemented according to the EMTP solution methodology. For comparison purpose, a state variable $qd0$ synchronous machine model [17] has also been implemented in MATLAB/Simulink. This model is solved using fourth-order Runge–Kutta method with a very small time step of 1 μs to obtain very accurate numerical solutions, which are used as reference. To demonstrate the improved numerical accuracy of the proposed CC-PD model over the conventional EMTP-type $qd0$ model, we used the build-in EMTP-RV's synchronous machine model as a benchmark case.

The salient-pole hydroturbine generator with parameters given in Appendix A has been used in all studies. To investigate the accuracy of the proposed PD model, one may consider a number of case studies, e.g., short-circuit of a fully loaded machine, a case of machine with large dynamic saliency, pole-slipping events, etc. However, such transient events excite mostly the low-frequency modes where the approximation introduced by additional fictitious damper winding should not have any visible impact. The transient studies of a three-phase fault have been previously considered in [8] and are not included here due to space limitations. Therefore, for the purpose of this paper, a single-phase-to-ground fault study is chosen as this even excites higher frequencies. In the following transient study, the generator initially operates with no load. At $t = 0.002$ s, a single-phase-to-ground fault is applied at the machine terminals (phase a). The transient responses produced by various models are plotted in Figs. 2–5. Such studies have been previously considered in [9] and may be very useful for benchmarking and/or validating various models.

A. Model Verification Using Small Time Step

The considered study of an unbalanced fault is first simulated using a relatively small time step, $\Delta t = 50$ μs. The resulting transients of the field current $i_{\rm fd}$, stator currents i_{as}, i_{bs}, and electromagnetic torque T_e are depicted in Fig. 2. The simulation results obtained by the EMTP-RV, the PD model [8], and the proposed CC-PD models are overlaid with the reference solutions. As can be observed from Fig. 2, the transient responses produced by all models coincide and converge to the reference solutions. This clearly demonstrates that these models are all equivalent and predict the unbalanced operations with acceptable accuracy for the given time step, which is an expected result.

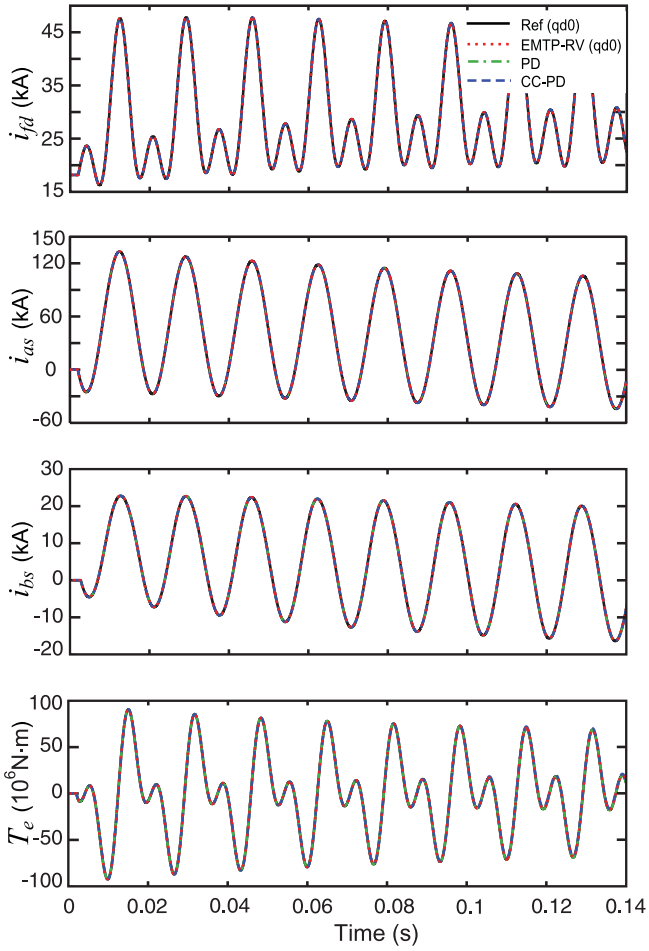

Fig. 2. Field and phase currents, and electromagnetic torque for the single-phase fault study using time step of 50 μs, as predicted by various models.

B. Model Verification Using Large Time Step

To further compare the numerical properties and robustness of the new CC-PD model, a larger time step, $\Delta t = 1$ ms, is applied to the same test case. The same variables are plotted in Figs. 3–5. As can be observed in Fig. 3, the results produced by the various models visibly diverge from the reference solution. The transient responses obtained by EMTP-RV($qd0$) model (red-dotted line) diverge from the reference solutions with the largest error among the considered models. The problem of convergence and accuracy of qd models is attributed to their interface with the external network and is discussed in detail in [8], [9], [22]. At the same time, the PD and CC-PD models still produce reasonably accurate and convergent simulation results.

A more detailed fragment of the transient observed in $i_{\rm fd}$ is shown in Fig. 4, which is a magnified view of Fig. 3 (first subplot). A magnified view of the phase current i_{bs} is shown in Fig. 5, which is a detailed view of Fig. 3 (third subplot). As Figs. 4 and 5 show, the point-by-point solutions obtained by the PD and CC-PD models are almost identical and are reasonably close to the reference solution. The detailed analysis of other variables shows similar result.

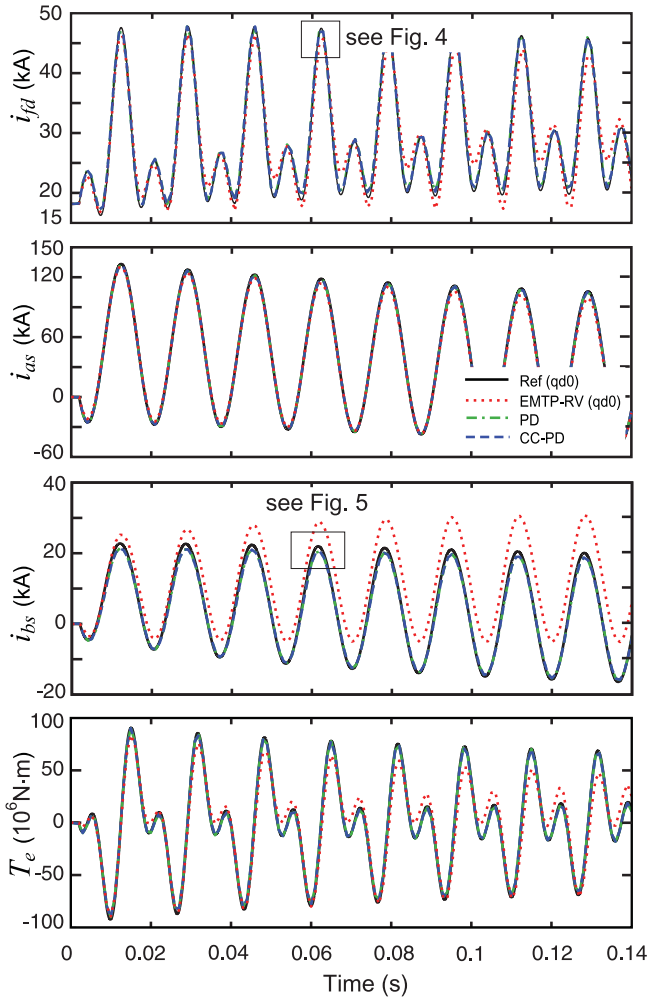

Fig. 3. Field and phase currents, and torque for the single-phase fault study using time step of 1 ms, as predicted by various models.

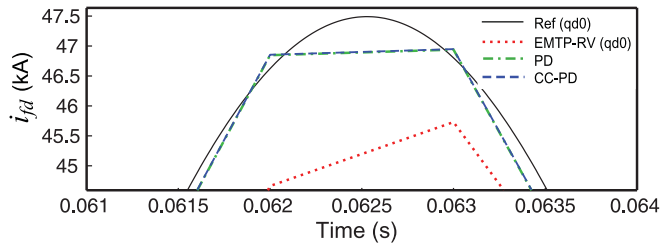

Fig. 4. Magnified view of field current for the single-phase fault study using time step of 1 ms, as predicted by various models.

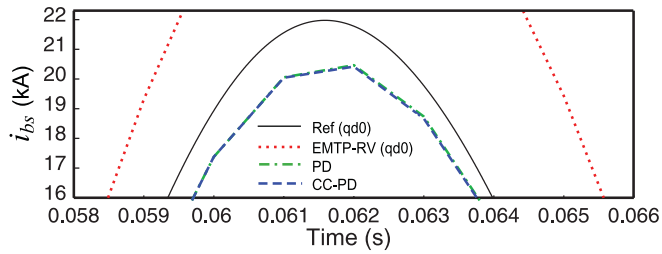

Fig. 5. Magnified view of phase b current for the single-phase fault study using time step of 1 ms, as predicted by various models.

VI. Discussion

A. Choice of Added Winding Parameters

The idea of adding a fictitious damper winding to eliminate the dynamic saliency was originated in [16]. This approach is used here for the proposed CC-PD model for EMTP-type solution. It is noted that Z_{lkqM+1} in (20) consists of two variables, R_{kqM+1} and L_{lkqM+1}, that need to be determined. These parameters should be determined subject to satisfying the constraint (23). At the same time, the q-axis frequency response in the low-frequency range should remain the same as it was in the original machine. Observing (20), one can see that for a given value of Z_{lkqM+1} [since (23) is a constraint], choosing smaller L_{lkqM+1} results in larger R_{kqM+1}. Also, as can be observed from (25), the larger winding resistance R_{kqM+1} makes the additional pole time constant τ_{QM+1} very small, which pushes the corner frequency of this pole far away from the fitting frequency $f_{\rm fit}$. Therefore, satisfying the inequality (28), and then choosing R_{kqM+1} according to (29), ensures that the added winding does not affect the machine's response in frequency domain as well as in time domain in the range of interest.

Interested reader can find very insightful discussions in [16] and [10] regarding the added winding parameter choice for implementing the synchronous machine model (in continuous time domain) for state-variable-based simulation packages. Therein, increasing the winding resistance R_{kqM+1}, although improves the model accuracy, also makes the machine model numerically stiff and possibly hard to solve/simulate, if an explicit integration method is used. However, for the EMTP solution, this does not represent a problem since the equations are discretized at the branch level using the implicit (stiffly stable) trapezoidal rule. So, in general, one can choose small L_{lkqM+1} to satisfy the constraint (28), and then choose very large resistance R_{kqM+1} so that the added winding effectively appear open-circuited, which minimizes its impact.

B. Model Accuracy

The PD model in general improves the numerical accuracy compared with the conventional $qd0$ models that are implemented in EMTP-RV, PSCAD, ATP/EMTP, etc. This is the result of the direct interface of the machine's stator circuit in abc phase coordinates with EMTP network solution. The proposed CC-PD model possesses the same interfacing accuracy as the conventional PD model. The detailed accuracy comparisons of various machine models, such as $qd0$, PD, and VBR, are documented in [8], [9], [21], and [22]. The numerical accuracy of the proposed CC-PD model is also verified by the simulation results in Figs. 2–5. Moreover, since the added damper winding has no effect (error) in steady state and only minimally impacts the transient response in very high frequencies due to relatively large value of the winding resistance, the proposed CC-PD model is expected to give very good results for most practical cases. The winding approximation is expected to give very good results for larger machines and the studies with predominantly slow transients that do not have high frequencies (e.g., three-phase faults, pole slipping of large generators, etc.).

The study presented in this paper demonstrates a single-phase-to-ground fault (which is richer in higher frequencies), wherein the proposed CC-PD model produces results that are almost identical to the conventional PD model even at relatively large time step (see Figs. 4 and 5). However, potentially, the area where the proposed CC-PD model may be less accurate could be, for example, small machines driven by switching converters (i.e. wherever the high-frequency transients are excited). For such cases, the fitting frequency $f_{\rm fit}$ will have to be increased according the needs of the study.

C. Network Solution Impact

Although the CC-PD model has slightly higher flop count per step (295 flops versus 251 flops, see Table II) than conventional PD, its major advantage is that it enables very efficient EMTP time stepping network solution. For the conventional PD model, the time-variant machine conductance submatrix forces the entire network $\mathbf{G}$ matrix to be refactorized at each time step. Although the use of sparse matrix techniques such as partial matrix factorization and optimal node ordering methods can alleviate the impact of the time-varying $\mathbf{G}$ matrix [23], [24], a constant conductance matrix is always preferred for efficient EMTP network solution. Interested reader can find case studies documented in [5] that compare the calculation times and the numbers of triangulations when using the conventional PD model and the classical *qd* model (Type-59 synchronous machine model in EMTP) with constant $\mathbf{G}$ matrix. Therein, for a 190-bus three-generator system, a ratio of 308.3/70.1 (about 4.4 times) of increased calculation time due to retriangulation was reported [5]. However, with the proposed CC-PD model, the need for retriangulation of the network $\mathbf{G}$ matrix is removed. At the same time, just like the conventional PD model, the CC-PD model preserves the direct interface of the machine electrical variables within the EMTP network solution. It is also understood that the computational speedup due to avoiding the network $\mathbf{G}$ matrix retriangulation will be system and case dependent. In general, the larger the power system network, the better simulation speedup from using the proposed CC-PD over the conventional PD model may be anticipated. These are indeed very interesting issues that would also shift the focus of publication toward power systems. Therefore, in the near future, the authors would like to take this issue to a separate dedicated publication in appropriate journal.

VII. Conclusion

In this paper, we have presented a new PD synchronous machine model for EMTP-type solution. The new model has a constant equivalent conductance matrix in the discrete-time machine–network interface equation, which is achieved by eliminating the dynamic saliency existing in the equivalent resistance matrix of the original PD model. This constant equivalent conductance matrix is desirable since it avoids the refactorization of the network conductance matrix at every time step. This feature may make the new model very attractive for possible use in various EMTP packages. A case study of salient-pole synchronous machine has been performed to demonstrate the effectiveness of the proposed constant equivalent conductance PD model. The large time step study has shown that the numerical accuracy of the proposed model is well preserved compared with the original PD model and represents significant improvement over the conventional *qd* models implemented in commercial EMTP-type software packages such as EMTP-RV.

Appendix A

Parameters of synchronous hydroturbine generator [17]: 325 MVA; 20 kV; 0.85 pf; 64 poles; 112.5 r/min; $H = 7.5$ s; $J = 35.1 \times 10^6$ kg·m^2; $\omega_b = 376.99$ rad/s.

Nominal circuit parameters: $R_s = 0.00234\ \Omega$; $X_{ls} = 0.1478\ \Omega$; $X_q = 0.5911\ \Omega$; $X_d = 1.0467\ \Omega$; $R_{fd} = 0.0005\ \Omega$; $X_{lfd} = 0.2523\ \Omega$; $R_{kd} = 0.01736\ \Omega$; $X_{lkd} = 0.1970\ \Omega$; $R_{kq1} = 0.01675\ \Omega$; $X_{lkq1} = 0.1267\ \Omega$.

Additional winding parameters:

1) fitted at $\Delta t = 50\ \mu$s: $R_{kq2} = 1{,}827.7\ \Omega$; $X_{lkq2} = 91.29\ \Omega$.
2) fitted at $\Delta t = 1000\ \mu$s: $R_{kq2} = 38.13\ \Omega$; $X_{lkq2} = 1.8081\ \Omega$.

Appendix B

Matrices and block submatrices used in the model:

$$\mathbf{R}_s = \text{diag}\,(\,R_s \quad R_s \quad R_s\,) \tag{B1}$$

$$\mathbf{R}_r = \text{diag}\lfloor\,\mathbf{R}_{rq} \quad \mathbf{R}_{rd}\,\rfloor = \text{diag}\lfloor\,\text{diag}\,(\,R_{kq1} \quad \cdots \quad R_{kqM}\,) \quad \text{diag}\,(\,R_{\rm fd} \quad R_{kd1} \quad \cdots \quad R_{kdN}\,)\,\rfloor \tag{B2}$$

$$\mathbf{L}_s(\theta_r) = \begin{bmatrix} L_{ls} + L_A - L_B\cos 2\theta_r & -\frac{1}{2}L_A - L_B\cos 2\left(\theta_r - \frac{\pi}{3}\right) & -\frac{1}{2}L_A - L_B\cos 2\left(\theta_r + \frac{\pi}{3}\right) \\ -\frac{1}{2}L_A - L_B\cos 2\left(\theta_r - \frac{\pi}{3}\right) & L_{ls} + L_A - L_B\cos 2\left(\theta_r - \frac{2\pi}{3}\right) & -\frac{1}{2}L_A - L_B\cos 2(\theta_r + \pi) \\ -\frac{1}{2}L_A - L_B\cos 2\left(\theta_r + \frac{\pi}{3}\right) & -\frac{1}{2}L_A - L_B\cos 2(\theta_r + \pi) & L_{ls} + L_A - L_B\cos 2\left(\theta_r + \frac{2\pi}{3}\right) \end{bmatrix} \tag{B3}$$

$$\text{where } L_A = \frac{L_{md} + L_{mq}}{3} \text{ and } L_B = \frac{L_{md} - L_{mq}}{3}. \tag{B4}$$

Mutual inductance matrices:

$$\mathbf{L}_{sr}(\theta_r) = \lfloor\, \mathbf{L}_{srq}(\theta_r) \quad \mathbf{L}_{srd}(\theta_r)\,\rfloor \text{ and } \mathbf{L}_{rs}(\theta_r) = \frac{2}{3}\left(\mathbf{L}_{sr}(\theta_r)\right)^T = \frac{2}{3}\begin{bmatrix}\mathbf{L}_{srq}(\theta_r)\\ \mathbf{L}_{srd}(\theta_r)\end{bmatrix} \tag{B5}$$

$$\text{where } \mathbf{L}_{srq}(\theta_r) = \begin{bmatrix} L_{mq}\cos\theta_r & \cdots & L_{mq}\cos\theta_r \\ L_{mq}\cos\left(\theta_r - \frac{2\pi}{3}\right) & \cdots & L_{mq}\cos\left(\theta_r - \frac{2\pi}{3}\right) \\ L_{mq}\cos\left(\theta_r + \frac{2\pi}{3}\right) & \cdots & L_{mq}\cos\left(\theta_r + \frac{2\pi}{3}\right) \end{bmatrix}_{3\times M}$$

$$\text{and } \mathbf{L}_{srq}(\theta_r) = \begin{bmatrix} L_{md}\sin\theta_r & \cdots & L_{md}\sin\theta_r \\ L_{md}\sin\left(\theta_r - \frac{2\pi}{3}\right) & \cdots & L_{md}\sin\left(\theta_r - \frac{2\pi}{3}\right) \\ L_{md}\sin\left(\theta_r + \frac{2\pi}{3}\right) & \cdots & L_{md}\sin\left(\theta_r + \frac{2\pi}{3}\right) \end{bmatrix}_{3\times(N+1)}. \tag{B6}$$

Rotor inductance matrix and its blocks:

$$\mathbf{L}_r = \text{diag}\,(\,\mathbf{L}_{rq} \quad \mathbf{L}_{rd}\,) \tag{B7}$$

$$\text{where } \mathbf{L}_{rq} = \begin{bmatrix} L_{lkq1}+L_{mq} & L_{mq} & \cdots & L_{mq} \\ L_{mq} & L_{lkq2}+L_{mq} & L_{mq} & \vdots \\ \vdots & L_{mq} & \ddots & L_{mq} \\ L_{mq} & \cdots & L_{mq} & L_{lkqM}+L_{mq} \end{bmatrix}_{M\times M}$$

$$\text{and } \mathbf{L}_{rd} = \begin{bmatrix} L_{lfd}+L_{md} & L_{md} & \cdots & L_{md} \\ L_{md} & L_{lkd1}+L_{md} & L_{md} & \vdots \\ \vdots & L_{md} & \ddots & L_{md} \\ L_{md} & \cdots & L_{md} & L_{lkdN}+L_{md} \end{bmatrix}_{(N+1)\times(N+1)} \tag{B8}$$

$$T_e = \frac{P}{2}\left\{\begin{array}{l} \frac{L_{md}-L_{mq}}{3}\left[\left(i_{as}^2 - \frac{1}{2}i_{bs}^2 - \frac{1}{2}i_{cs}^2 - i_{as}i_{bs} - i_{as}i_{cs} - i_{bs}i_{cs}\right)\sin(2\theta_r)\right. \\ \quad \left. + \frac{\sqrt{3}}{2}\left(i_{bs}^2 - i_{cs}^2 - 2i_{as}i_{bs} + 2i_{as}i_{cs}\right)\cos(2\theta_r)\right] \\ -L_{mq}\left(\sum_{x=1}^{M} i_{kqx}\right)\left[\left(i_{as} - \frac{1}{2}i_{bs} - \frac{1}{2}i_{cs}\right)\sin(\theta_r) - \frac{\sqrt{3}}{2}\left(i_{bs} - i_{cs}\right)\cos(\theta_r)\right] \\ \quad + L_{md}\left(i_{fd} + \sum_{x=1}^{N} i_{kdx}\right)\left[\left(i_{as} - \frac{1}{2}i_{bs} - \frac{1}{2}i_{cs}\right)\cos(\theta_r) + \frac{\sqrt{3}}{2}\left(i_{bs} - i_{cs}\right)\sin(\theta_r)\right] \end{array}\right\}. \tag{B9}$$

APPENDIX C

Theorem 1: For synchronous machine with arbitrary number of damper windings, the equivalent resistance matrix $\mathbf{R}_{\text{eq}}^{pd}$ can be expressed in the form of (12).

Proof: Without loss of generality, a synchronous machine with two damping windings *kq1*, *kq2* in q-axis, one field winding *fd* and one damping winding *kd* in d-axis is assumed. The proof goes through the following five steps:

Step 1: The triple matrix product in (7) is reformulated using the machine resistance and inductance matrices (B2), (B5)–(B8) into two separate parts, for q- and d-axis components as

$$\mathbf{L}_{sr}(t)\left(\mathbf{R}_r + \frac{2}{\Delta t}\mathbf{L}_r\right)^{-1}\mathbf{L}_{rs}(t) = \mathbf{L}_{srq}(t)\left(\mathbf{R}_{rq} + \frac{2}{\Delta t}\mathbf{L}_{rq}\right)^{-1}\mathbf{L}_{rsq}(t) + \mathbf{L}_{srd}(t)\left(\mathbf{R}_{rd} + \frac{2}{\Delta t}\mathbf{L}_{rd}\right)^{-1}\mathbf{L}_{rsd}(t). \tag{C1}$$

Step 2: The matrix inverse in the first term (the q-axis term) of (C1) can be expressed as

$$\left(\mathbf{R}_{rq}+\frac{2}{\Delta t}\mathbf{L}_{rq}\right)^{-1}=\begin{bmatrix} Z_{lkq1}+Z_{mq} & Z_{mq} \\ Z_{mq} & Z_{lkq2}+Z_{mq}\end{bmatrix}^{-1}. \tag{C2}$$

The matrix inverse of (C2) can be further solved using Theorem 2 in Appendix D as

$$\begin{bmatrix} Z_{lkq1}+Z_{mq} & Z_{mq} \\ Z_{mq} & Z_{lkq2}+Z_{mq}\end{bmatrix}^{-1}=\begin{bmatrix} \dfrac{1+Z_{mq}Z_{lkq2}^{-1}}{Z_{lkq1}D_{2q}} & -\dfrac{Z_{mq}}{Z_{lkq1}Z_{lkq2}D_{2q}} \\ -\dfrac{Z_{mq}}{Z_{lkq2}Z_{lkq1}D_{2q}} & \dfrac{1+Z_{mq}Z_{lkq1}^{-1}}{Z_{lkq2}D_{2q}}\end{bmatrix} \tag{C3}$$

$$\text{where } D_{2q}=1+\frac{Z_{mq}}{Z_{lkq\Sigma 2}} \text{ and } Z_{lkq\Sigma 2}=((Z_{lkq1})^{-1}+(Z_{lkq2})^{-1})^{-1}. \tag{C4}$$

Using (C2)–(C4), the first term of (C1) can be expressed as

$$\begin{aligned}&\mathbf{L}_{srq}(t)\left(\mathbf{R}_{rq}+\frac{2}{\Delta t}\mathbf{L}_{rq}\right)^{-1}\mathbf{L}_{rsq}(t)\\ &=\frac{2}{3}\frac{L_{mq}^2}{Z_{kq\Sigma 2}+Z_{mq}}\begin{bmatrix} \cos^2\theta_r & \cos\theta_r\cos\left(\theta_r-\frac{2\pi}{3}\right) & \cos\theta_r\cos\left(\theta_r+\frac{2\pi}{3}\right) \\ \cos\left(\theta_r-\frac{2\pi}{3}\right)\cos\theta_r & \cos^2\left(\theta_r-\frac{2\pi}{3}\right) & \cos\left(\theta_r-\frac{2\pi}{3}\right)\cos\left(\theta_r+\frac{2\pi}{3}\right) \\ \cos\left(\theta_r+\frac{2\pi}{3}\right)\cos\theta_r & \cos\left(\theta_r+\frac{2\pi}{3}\right)\cos\left(\theta_r-\frac{2\pi}{3}\right) & \cos^2\left(\theta_r+\frac{2\pi}{3}\right)\end{bmatrix}.\end{aligned} \tag{C5}$$

Step 3: The similar procedure is applied for the second term of (C1) (the d-axis term). The matrix inverse of the second term in (C1) is expressed as

$$\left(\mathbf{R}_{rd}+\frac{2}{\Delta t}\mathbf{L}_{rd}\right)^{-1}=\begin{bmatrix} Z_{lfd}+Z_{md} & Z_{md} \\ Z_{md} & Z_{lkd}+Z_{md}\end{bmatrix}^{-1}=\begin{bmatrix} \dfrac{1+Z_{md}Z_{lkd}^{-1}}{Z_{lfd}D_{2d}} & -\dfrac{Z_{md}}{Z_{lfd}Z_{lkd}D_{2d}} \\ -\dfrac{Z_{md}}{Z_{lkd}Z_{lfd}D_{2d}} & \dfrac{1+Z_{md}Z_{lfd}^{-1}}{Z_{lkd}D_{2d}}\end{bmatrix} \tag{C6}$$

$$\text{where } D_{2d}=1+\frac{Z_{md}}{Z_{lkd\Sigma 2}} \text{ and } Z_{lkd\Sigma 2}=((Z_{lfd})^{-1}+(Z_{lkd})^{-1})^{-1}. \tag{C7}$$

Using (C6) and (C7), the second term of (C1) can be expressed as

$$\begin{aligned}&\mathbf{L}_{srd}(t)\left(\mathbf{R}_{rd}+\frac{2}{\Delta t}\mathbf{L}_{rd}\right)^{-1}\mathbf{L}_{rsd}(t)\\ &=\frac{2}{3}\frac{L_{md}^2}{Z_{kd\Sigma 2}+Z_{md}}\begin{bmatrix} \sin^2\theta_r & \sin\theta_r\sin\left(\theta_r-\frac{2\pi}{3}\right) & \sin\theta_r\sin\left(\theta_r+\frac{2\pi}{3}\right) \\ \sin\left(\theta_r-\frac{2\pi}{3}\right)\sin\theta_r & \sin^2\left(\theta_r-\frac{2\pi}{3}\right) & \sin\left(\theta_r-\frac{2\pi}{3}\right)\sin\left(\theta_r+\frac{2\pi}{3}\right) \\ \sin\left(\theta_r+\frac{2\pi}{3}\right)\sin\theta_r & \sin\left(\theta_r+\frac{2\pi}{3}\right)\sin\left(\theta_r-\frac{2\pi}{3}\right) & \sin^2\left(\theta_r+\frac{2\pi}{3}\right)\end{bmatrix}.\end{aligned} \tag{C8}$$

Step 4: For the purpose of model derivation, the triple matrix product in the equivalent resistance matrix (7) is defined as a new matrix $\mathbf{A}$.

$$\mathbf{L}_{sr}(t)\left(\mathbf{R}_{r}+\frac{2}{\Delta t}\mathbf{L}_{r}\right)^{-1}\mathbf{L}_{rs}(t)=\mathbf{A}=\begin{bmatrix} a_{11} & a_{12} & a_{13} \\ a_{21} & a_{22} & a_{23} \\ a_{31} & a_{32} & a_{33}\end{bmatrix}. \tag{C9}$$

Using (C5) and (C8), the elements of $\mathbf{A}$ can be represented in terms of machine parameters. Without loss of generality, the first element a_{11} is expressed here as an example

$$a_{11} = \frac{2}{3}\frac{L_{mq}^2}{Z_{kq\Sigma 2} + Z_{mq}}\cos^2\theta_r + \frac{2}{3}\frac{L_{md}^2}{Z_{kd\Sigma 2} + Z_{md}}\sin^2\theta_r. \tag{C10}$$

Substituting the trigonometric identity, $\sin^2\theta_r = 1 - \cos^2\theta_r$, the coefficient a_{11} can be expressed as

$$a_{11} = \frac{2}{3}\left(\frac{L_{mq}^2}{Z_{kq\Sigma 2} + Z_{mq}} - \frac{L_{md}^2}{Z_{kd\Sigma 2} + Z_{md}}\right)\cos^2\theta_r + \frac{2}{3}\frac{L_{md}^2}{Z_{kd\Sigma 2} + Z_{md}}. \tag{C11}$$

Step 5: The constant and rotor-position-dependent terms in the equivalent resistance matrix $\mathbf{R}_{\text{eq}}^{pd}(t)$ can be separated by substituting (B3) and (C9) into (7). The rotor-position-dependent terms can be combined and further simplified. Without loss of generality, as an example, the rotor-position-dependent term $r_{11}(t)$ in the first element of $\mathbf{R}_{\text{eq}}^{pd}(t)$ is expressed as

$$R_{11}(t) = -\frac{2}{\Delta t}L_B\cos 2\theta_r - \frac{2}{3}\left(\frac{2}{\Delta t}\right)^2\left(\frac{L_{mq}^2}{Z_{kq\Sigma 2} + Z_{mq}} - \frac{L_{md}^2}{Z_{kd\Sigma 2} + Z_{md}}\right)\cos^2\theta_r. \tag{C12}$$

Substituting the trigonometric identity $\cos^2\theta_r = \frac{1+\cos 2\theta_r}{2}$ into (C12), $R_{11}(t)$ can be expressed as

$$R_{11}(t) = -\frac{2}{\Delta t}\frac{L_{md} - L_{mq}}{3}\cos 2\theta_r - \frac{2}{3}\left(\frac{2}{\Delta t}\right)^2\left(\frac{L_{mq}^2}{Z_{kq\Sigma 2} + Z_{mq}} - \frac{L_{md}^2}{Z_{kd\Sigma 2} + Z_{md}}\right)\frac{1+\cos 2\theta_r}{2}. \tag{C13}$$

The rotor-position-dependent terms in (C13) can be collected as

$$\begin{aligned} R'_{11}(t) &= -\frac{2}{\Delta t}\frac{L_{md} - L_{mq}}{3}\cos 2\theta_r - \frac{1}{3}\left(\frac{2}{\Delta t}\right)^2\left(\frac{L_{mq}^2}{Z_{kq\Sigma 2} + Z_{mq}} - \frac{L_{md}^2}{Z_{kd\Sigma 2} + Z_{md}}\right)\cos 2\theta_r \\ &= \frac{1}{3}\left(\frac{Z_{kq\Sigma 2}Z_{mq}}{Z_{kq\Sigma 2} + Z_{mq}} - \frac{Z_{kd\Sigma 2}Z_{md}}{Z_{kd\Sigma 2} + Z_{md}}\right)\cos 2\theta_r = \frac{1}{3}\left(Z''_q - Z''_d\right)\cos 2\theta_r. \end{aligned} \tag{C14}$$

It is observed in (C14) that $R'_{11}(t)$ is the same as the rotor-position-dependent term in the first element of the equivalent resistance matrix (12). The same procedure and conclusion apply to all other elements in the variable term in (12), which completes the proof.

APPENDIX D

Theorem 2: The analytical inverse of a special matrix (that has self inductances in diagonal and the same mutual inductances in all off diagonal entries) has the following form:

$$\begin{aligned} &\begin{bmatrix} Z_{lkq1} + Z_{mq} & Z_{mq} & \cdots & Z_{mq} \\ Z_{mq} & Z_{lkq2} + Z_{mq} & \cdots & Z_{mq} \\ \vdots & \vdots & \ddots & \vdots \\ Z_{mq} & Z_{mq} & \cdots & Z_{lkqN} + Z_{mq} \end{bmatrix}_{M\times M}^{-1} \\ &= \begin{bmatrix} \dfrac{1 + Z_{mq}(Z_{lkq\Sigma M}^{-1} - Z_{lkq1}^{-1})}{Z_{lkq1}D_{Mq}} & -\dfrac{Z_{mq}}{Z_{lkq1}Z_{lkq2}D_{Mq}} & \cdots & -\dfrac{Z_{mq}}{Z_{lkq1}Z_{lkqM}D_{Mq}} \\ -\dfrac{Z_{mq}}{Z_{lkq2}Z_{lkq1}D_{Mq}} & \dfrac{1 + Z_{mq}(Z_{lkq\Sigma M}^{-1} - Z_{lkq2}^{-1})}{Z_{lkq2}D_{Mq}} & \cdots & -\dfrac{Z_{mq}}{Z_{lkq2}Z_{lkqM}D_{Mq}} \\ \vdots & \vdots & \ddots & \vdots \\ -\dfrac{Z_{mq}}{Z_{lkqM}Z_{lkq1}D_{Mq}} & -\dfrac{Z_{mq}}{Z_{lkqM}Z_{lkq2}D_{Mq}} & \cdots & \dfrac{1 + Z_{mq}(Z_{lkq\Sigma M}^{-1} - Z_{lkqM}^{-1})}{Z_{lkqM}D_{Mq}} \end{bmatrix}_{M\times M} \end{aligned} \tag{D1}$$

$$\text{where } D_{Mq} = 1 + \frac{Z_{mq}}{Z_{lkq\Sigma M}} \text{ and } Z_{lkq\Sigma M} = \left(\sum_{j=1}^{N}(Z_{lkqj})^{-1}\right)^{-1}. \tag{D2}$$

Note: It can be shown that using step-by-step row and column reductions one can obtain the result (D1). The detailed proof is not included in Appendix D due to space limitation.

REFERENCES

[1] H. W. Dommel, *EMTP Theory Book*. Vancouver, BC, Canada: MicroTran Power System Analysis Corp., May 1992.

[2] *Simulink Dynamic System Simulation Software—Users Manual*, MathWorks, Natick, MA, 2012.

[3] O. Wasynczuk and S. D. Sudhoff, "Automated state model generation algorithm for power circuits and systems," *IEEE Trans. Power Syst.*, vol. 11, no. 4, pp. 1951–1956, Nov. 1996.

[4] J. R. Marti and K. W. Louie, "A phase-domain synchronous generator model including saturation effects," *IEEE Trans. Power Systems*, vol. 12, no. 1, pp. 222–229, Feb. 1997.

[5] X. Cao, A. Kurita, H. Mitsuma, Y. Tada, and H. Okamoto, "Improvements of numerical stability of electromagnetic transient simulation by use of phase-domain synchronous machine models," *Electr. Eng. Jpn.*, vol. 128, no. 3, pp. 53–62, Apr. 1999.

[6] A. B. Dehkordi, A. M. Gole, and T. L. Maguire, "Permanent magnet synchronous machine model for real-time simulation," presented at the Interracial Conf. Power Syst. Transients, Montreal, QC, Canada, Jun. 2005.

[7] S. D. Pekarek, O. Wasynczuk, and H. J. Hegner, "An efficient and accurate model for the simulation and analysis of synchronous machine/converter systems," *IEEE Trans. Energy Convers.*, vol. 13, no. 1, pp. 42–48, Mar. 1998.

[8] L. Wang and J. Jatskevich, "A voltage-behind-reactance synchronous machine model for the EMTP-type solution," *IEEE Trans. Power Syst.*, vol. 21, no. 4, pp. 1539–1549, Nov. 2006.

[9] L. Wang, J. Jatskevich, and H. W. Dommel, "Reexamination of synchronous machine modeling techniques for electromagnetic transient simulations," *IEEE Trans. Power Syst.*, vol. 22, no. 3, pp. 1221–1230, Aug. 2007.

[10] M. Chapariha, L. Wang, J. Jatskevich, H. Dommel, and S. D. Pekarek, "Constant parameter RL-branch equivalent circuit for interfacing AC machine models in state-variable-based simulation packages," *IEEE Trans. Energy Convers.*, vol. 27, no. 3, pp. 634–645, Sep. 2012.

[11] *MicroTran Reference Manual* (1997). MicroTran Power System Analysis Corp., Vancouver, BC, Canada, [Online]. Available: http://www.microtran.com

[12] *Alternative Transients Programs* (2007). ATP-EMTP, ATP User Group, West Linn, OR, [Online]. Available: http://www.emtp.org

[13] *PSCAD/EMTDC* (2007). Manitoba HVDC Research Centre and RTDS Technologies Inc., Winnipeg, MB, Canada, [Online]. Available: http://www.pscad.com

[14] *Electromagnetic Transient Program* (2007). EMTP RV, CEA Technologies Inc., Columbia, MD, [Online]. Available: http://www.emtp.com

[15] L. Wang and J. Jatskevich, "Approximate voltage-behind-reactance induction machine model for efficient interface with EMTP network solution," *IEEE Trans. Power Syst.*, vol. 25, no. 2, pp. 1016–1031, May 2010.

[16] S. D. Pekarek and E. A. Walters, "An accurate method of neglect dynamic saliency of synchronous machines in power electronic based systems," *IEEE Trans. Energy Convers.*, vol. 14, no. 4, pp. 1177–1183, Dec. 1999.

[17] P. C. Krause, O. Wasynczuk, and S. D. Sudhoff, *Analysis of Electric Machine*, 2nd ed. Piscataway, NJ: IEEE Press, 2002.

[18] V. Brandwajn, "Synchronous generator models for the analysis of electromagnetic transients," Ph.D. dissertation, Univ. British Columbia, Vancouver, BC, Canada, 1977.

[19] T. Ito and S. Kojima, "Inaccuracies of trigonometric functions in computer mathematical libraries," *Publ. Nat. Astronom. Observ. Jpn.*, vol. 8, no. 1–4, pp. 17–31, 2005.

[20] S. Boyd and L. Vandenberghe, *Convex Optimization*. Cambridge, U.K.: Cambridge Univ. Press, 2004, pp. 662–664.

[21] L. Wang, J. Jatskevich, C. Wang, and P. Li, "A voltage-behind-reactance induction machine model for the EMTP-type solution," *IEEE Trans. Power Systems*, vol. 23, no. 3, pp. 1226–1238, Aug. 2008.

[22] L. Wang, J. Jatskevich, V. Dinavahi, H. W. Dommel, J. A. Martinez, K. Strunz, M. Rioual, G. W. Chang, and R. Iravani, "Methods of interfacing rotating machine models in transient simulation programs," *IEEE Trans. Power Del.*, vol. 25, no. 2, pp. 891–903, Apr. 2010.

[23] H. W. Dommel, "Nonlinear and time-varying elements in digital simulation of electromagnetic transients," *IEEE Trans. Power App. Syst.*, vol. PAS-90, no. 2, pp. 2561–2567, Nov./Dec. 1971.

[24] S. M. Chan and V. Brandwajn, "Partial matrix refactorization," *IEEE Trans. Power App. Syst.*, vol. PWRS-1, no. 1, pp. 193–200, Feb. 1986.

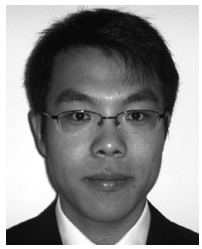

Liwei Wang (S'04–M'10) received the M.S. degree in electrical engineering from Tianjin University, Tianjin, China, and the Ph.D. degree in electrical and computer engineering from the University of British Columbia, Vancouver, BC, Canada, in 2004 and 2010, respectively.

From February 2009 to July 2009, he was an Internship Researcher at ABB Corporate Research Center, Baden-Dattwil, Switzerland. He was a Postdoctoral Research Fellow in the Department of Electrical and Computer Engineering, University of British Columbia from February 2010 to July 2010. In August 2010, he joined ABB Corporate Research Center, Västerås, Sweden, as a Research Scientist. He is a holder of nine patent filings in the area of high power electronic converter topologies and high-power converter designs. His research interests include power system analysis, operation and simulation, electrical machine and drives, power electronic converter design, control and topology, power semiconductors modeling and characterization, utility power electronics applications, HVDC and FACTS, renewable energy sources, and distributed generation.

Juri Jatskevich (M'99–SM'07) received the M.S.E.E. and Ph.D. degrees in electrical engineering from Purdue University, West Lafayette, IN, in 1997 and 1999, respectively.

Since 2002, he has been a Faculty Member at the University of British Columbia, Vancouver, BC, Canada, where he is currently a Professor of Electrical and Computer Engineering. He chaired the IEEE CAS Power Systems & Power Electronic Circuits Technical Committee in 2009–2010. His research interests include power electronic systems, electrical machines and drives, and modeling and simulation of electromagnetic transients.

Dr. Jatskevich is currently an Editor of the IEEE TRANSACTIONS ON ENERGY CONVERSION, Editor of IEEE POWER ENGINEERING LETTERS, and Associate Editor of IEEE TRANSACTIONS ON POWER ELECTRONICS. He is also chairing the IEEE Task Force on Dynamic Average Modeling, under Working Group on Modeling and Analysis of System Transients Using Digital Programs.